NETmix®, A New Type of Static Mixer: Modeling, Simulation, Macromixing, and Micromixing Characterization

Paulo E. Laranjeira, António A. Martins, José Carlos B. Lopes, and Madalena M. Dias
Laboratory of Separation and Reaction Engineering, Departamento de Engenharia Química, Faculdade de Engenharia da Universidade do Porto, Rua Dr. Roberto Frias, 4200-465 Porto, Portugal

DOI 10.1002/aic.11815
Published online July 7, 2009 in Wiley InterScience (www.interscience.wiley.com).

NETmix® is a new technology for static mixing based on a network of chambers connected by channels. The NETmix® model is the basis of a flow simulator coupled with chemical reaction used to characterize macro and micromixing in structured porous media. The chambers are modeled as perfectly mixing zones and the channels as plug flow perfect segregation zones. A segregation parameter is introduced as the ratio between the channels volume and the whole network volume. Different kinetics and reactants injection schemes can be implemented. Results show that the number of rows in the flow direction and the segregation parameter control both macro and micromixing, but the degree of micromixing is also controlled by the reactants injection scheme. The NETmix® model enables the systematic study of micromixing and macromixing for different network structures and reaction schemes, enabling the design of network structures to ensure the desired yield and selectivity. © 2009 American Institute of Chemical Engineers *AIChE J,* 55: 2226–2243, 2009

Keywords: mixing, network models, porous media, static mixers

Introduction

The importance of mixing can hardly be exaggerated. Mixing is at the heart of many operations in the chemical, petrochemical, and pharmaceutical process industries, and is often accompanied by chemical reactions whose outcome depends strongly upon the efficiency of the mixing process.[1,2] Examples include chemical reactors, dispersion, and transport of contaminants in porous media, among many other examples.[3,4] Therefore, a computationally efficient mathematical model capable of predicting mixing and chemical reaction is clearly desirable for the design of process equipment such as static mixers.[5]

Network models have been widely adopted as a basis for describing the void structure and transport properties of porous media for over 40 years. A network model is intuitively desirable, because it avoids a detailed geometric description of the void space in favor of an idealized description that is amenable to a computational and even a analytical treatment. The concept that fluid paths in a porous medium may split and, later on, join other paths, has prompted most authors to think of a network model of pore space in which the branches represent the pore throats or the narrow channels that connect the nodes that represent the pore bodies. Many authors ignore nodes and assign them no volume, although there have been several papers in which this assumption has been relaxed,[6–8] and currently it is even considered that most of the void space of a porous medium is associated not with the network branches but with the nodes.[9]

One of the earliest attempts of using network models to model flow through a porous medium was the work of Fatt (1956).[10] Network models were later used to predict the macroscopic transport and capillary equilibrium properties of porous media, for example: simulation of mercury intrusion porosimetry curves of sandstones and catalyst particles;[11–14] prediction of air-mercury and oil-water drainage capillary

Correspondence concerning this article should be addressed to M. M. Dias at dias@fe.up.pt

curves[11,15] and relative permeability curves of sandstones;[16] study of two-phase flow immiscible displacement at finite capillary numbers,[17–20] and single phase flow through in porous media.[21,22] Other authors also used network models to describe flow and dispersion in porous media, without reaction,[23–26] or with the inclusion of adsorption[27,28] or chemical reaction.[29,30] Network models were also used to describe quantitatively the mass transfer and sorption mechanisms occurring in porous adsorbent particles and monoliths packed columns,[31,32] and more recently, to model the mass transport and chemical reaction in packed bed reactors for the isomerization of glucose considering the deactivation of immobilized glucose isomerase and how the behavior at particle level influences the macroscopic performance of the reactor,[33–35] and to study the scaling effects of geochemical reactions when adjusting the results obtained at bench laboratory to real porous media.[36] Also available in the open literature are models, such as the PHREEC model,[37] implemented in simulation software. However, this model is somewhat difficult to use and it is based on data that can be hard or even impossible to obtain, such as the parameters for statistical models that describe the local structure of the porous media.

Research on mixing in stirred vessel reactors conducted to the development of the networks-of-zones model, based on a network of perfectly mixed interconnected zones. Its application includes: description of mixing in fixed beds of spheres[38] and fixed bed reactors,[39] tracer dispersion and mixing in stirred reactors,[40,41] and gas dispersion in stirred gas–liquid reactors.[42] Recent works have further adopted the networks-of-zones model as a basis to study gas–liquid bioreactors,[43] multiple-impeller operation,[44] and to predict the semibatch selectivity in products for multiple reactions.[45,46]

The analysis of the literature shows that only through a detailed description of the transport phenomena at the microscopic level (e.g., at least at the particle scale) it is possible to obtain an adequate description of the observed macroscopic behavior of a static mixer and a porous medium. In recent years, there is an increased interest for structured process in which it is possible to control the relevant transport processes, leading to significant improvements over traditional process in many cases.[47] So, the study of transport phenomena in porous media and static mixers is very relevant from an economical, and in more recent years, from a environmental point of view, because it makes it possible to improve the material and energy efficiency of existing or new processes, or even of new one. A promising approach involves the development of new modeling and simulation tools, based on the description of the relevant characteristics of the structural characteristics at the local level, and the significant physical phenomena, and how it affects the macroscopic behavior.

NETmix® is a new kind of static mixer[48] whose genesis is a network model of chambers and channels developed initially to describe and simulate laminar and turbulent flows[22] and transport phenomena[49] in porous media. This model was then extended using a network-of-zones to simulate chemical reaction and characterize macro and micromixing. The model, referred as the NETmix® model, is described and studied in this work. The exceptional mixing qualities of this type of structure led to development of a static mixer protected by an international patent application.[50]

The predictions of the NETmix® model have been compared with experimental data obtained in a specially designed two dimensional experimental unit.[48]

Model Description

In the NETmix® model, a network structure determines the overall flow patterns and thus the distribution of residence times as a probe to the characterization of macromixing. Here the network structure is described as well as the methodology for determining the hydrodynamics inside the generated network. A chemical reaction simulator used for micromixing characterization based on a network-of-zones model simulator is described next.

Network structure

The NETmix® model consists of a network structure that combines in a structured manner two different types of elements—chambers and channels—organized in a 2D (bidimensional) network. This is a realistic form of representing the local structure of a real porous medium, in particular packed beds, that can seen qualitatively as larger voids, described as spheres and characterized by their diameter, interconnected by smaller voids, depicted as cylinders, and describe by their diameter and length. The process of generating the 2D network is described in detail in Martins et al. (2007).[22] Here a short description is presented for the sake of completeness.

The network is generated by the repetition of a unit cell, shown in Figure 1a. The direction of the flow is assumed to follow the x-axis. Thus, the channels normal to the x-axis are denoted horizontal channels (HC), while the remaining channels, forming an angle ϕ with the x-axis, are denoted oblique channels (OC). Each chamber is modeled as a sphere with diameter D_j and each channel is modeled as a cylinder with diameter d_i and length l_i.

Unit cells are repeated and connected through both the horizontal and the oblique channels by fixing the distance between the centers of obliquely interconnected chambers, L^o, as shown in Figure 1b. The network size is specified by the number of unit cells in the x and y directions, that is, the number of rows and columns, n_x and n_y, respectively. Adding exit channels to the last row of chambers completes the two-dimensional network generation (see Figure 1b).

The model includes the possibility of generating various types of networks. The network coordination number (number of channels connected to each chamber) can be varied by generating networks with horizontal channels (HC), Figures 2a,b, or without horizontal channels, Figures 2c,d, resulting in coordination numbers of 6 and 4, respectively. It is also possible to simulate two different types of boundary conditions: periodic and nonperiodic. Periodic boundary conditions (PBC) are simulated by connecting the boundary channels to the respective chambers on the network opposite, Figures 2a,c, and the network can be considered as a small fraction of an infinitely large medium. A finite medium is simulated using nonperiodic boundary conditions (NPBC) by removing the boundary channels on both sides of the network as shown in Figures 2b,d.

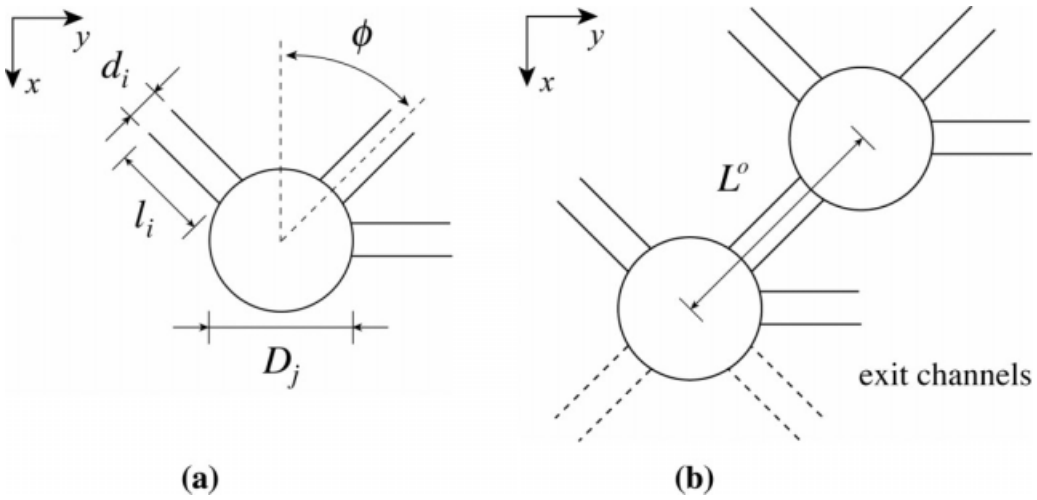

Figure 1. (a) Network unit cell; (b) two unit cells connected, showing the additional exit channels.

The model further includes the possibility of generating regular networks where both the channel and chamber diameters are constant (Figures 2a through d), or random-sized networks, where both the channel and chamber diameters vary randomly (Figure 2e).

With respect to the network structure the model furthermore includes the additional possibility of removing chambers and or channels in a random or specified manner, and thus encompassing the adjustment to different specific situations, namely to obtain networks with specified average coordination numbers (Figure 2f).

For the network structure to be macroscopically defined, the parameters n_x and n_y, the dimension L^o and the angle ϕ must be defined. The local structure is then assessed by selecting the type of boundary conditions (PBC or NPBC) and the presence or not of HC, and setting the average dimensions of the two types of elements and the respective size distributions (regular or random sized).

Regular networks are generated by assigning to all channels and chambers uniform diameter values, d and D, respectively. Random-sized networks are generated by randomly assigning the channels and chambers diameters, d_i and D_j, values following prespecified size distributions. In both cases, regular or random-sized networks, it is also imposed that the diameter of any chamber is larger than the diameter of the channels associated with it.

Hydrodynamics

The hydrodynamic model purpose is the simulation of single-phase flow in laminar regime in order to obtain the pressure field and the flow map inside the network. The following assumptions were considered:

- incompressible, isothermal, and steady state flow;
- perfectly mixed chambers, with no flow resistance at the interface between chamber and channel;
- piston flow in the channels;
- negligible gravitational effects;
- negligible pressure drop resulting from the sudden contraction and expansion of flow area in the channels and chambers intersections.[22]

According to the results of the Martins et al. (2007),[22] this last assumption is strictly valid for low Reynolds number, corresponding to conditions of creeping flow. Although some differences were observed between the flow fields for linear and nonlinear flow regimes, these differences are small and are not expected to change significantly the behavior of the NETmix® model and the nature of the mechanisms that control macro and micromixing.

Further, it is assumed that the n_y network inlet chambers are connected through the inlet channels to a reservoir of fluid at pressure P_1, whereas the n_y network outlet chambers are connected through the outlet channels to a sink of pressure P_0 (for simplicity $P_0 = 0$). The imposed pressure difference is then

$$\Delta p_T = P_1 - P_0 \tag{1}$$

The flow hydrodynamics is simulated using an analogy to a pure resistive electrical circuit, where the flow rate through the channels, q_i, and the pressure inside the chambers, p_j, correspond to the current across the resistance branches i and to the voltage in the nodes j, respectively.[18] The mass conservation equation for the network chamber j is given by

$$\sum_k q_{i_k} = 0 \tag{2}$$

where q_{i_k} is the flow rate in each channel i_k connected to chamber j. From Ohm's law, the pressure drop across a channel i is

$$\Delta p_i = p_{j_m} - p_{j_n} = R_i q_i \tag{3}$$

where R_i is the hydraulic resistance associated with channel i, q_i is the flow rate through channel i, and p_{j_m} and p_{j_n} are the pressures of the two chambers, j_m and j_n, connected to channel, i.

Because in this work pressure drop calculations take only into account the frictional effects on the channels walls, the hydraulic resistance is given by

$$R_i = \frac{128 \mu l_i}{\pi d_i^4} \tag{4}$$

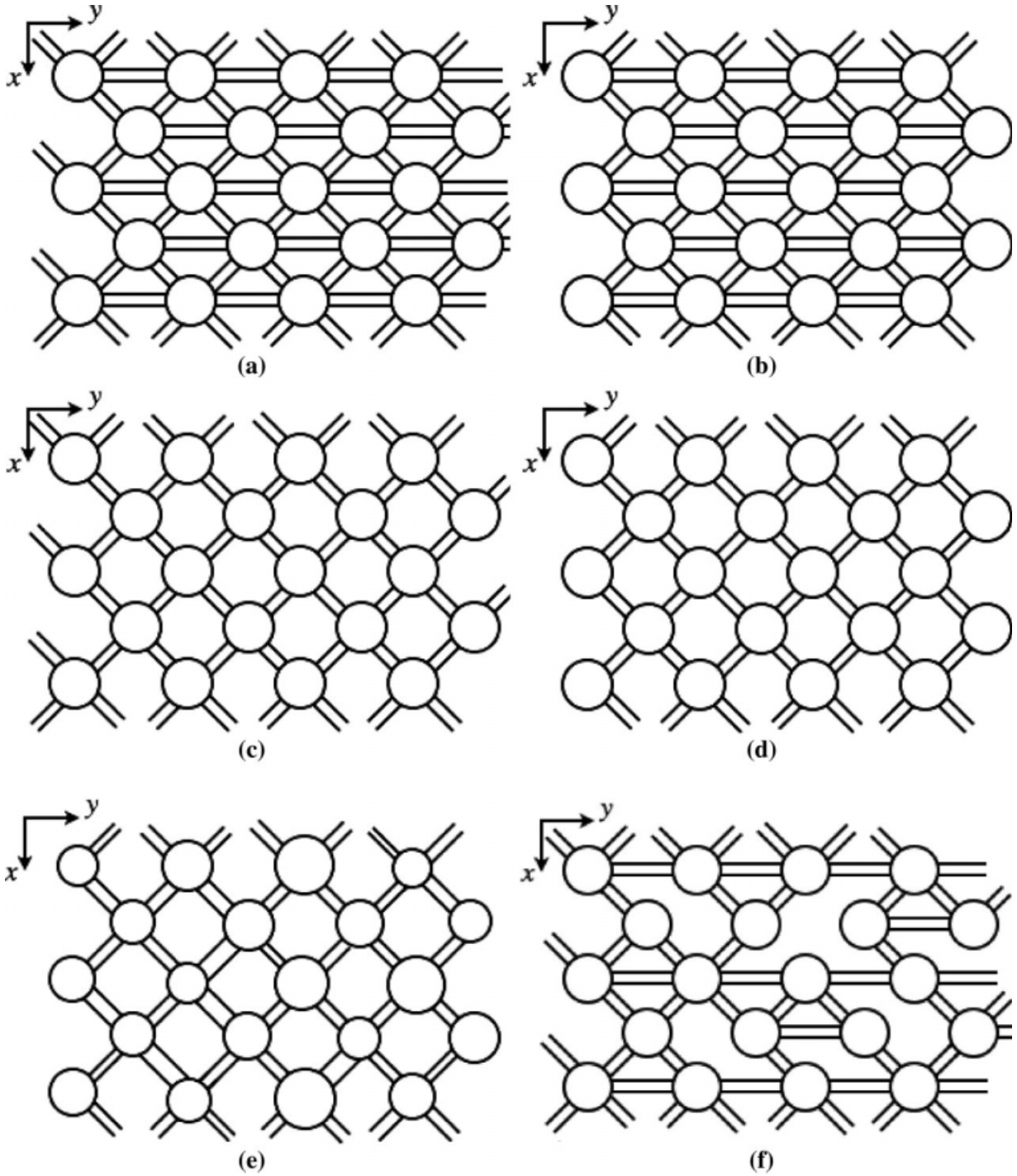

Figure 2. Examples of different types of $n_x = 5$ and $n_y = 4$ networks: (a) Regular network, PBC, with HC; (b) Regular network, NPBC, with HC; (c) Regular network, PBC, without HC; (d) Regular network, NPBC, without HC; (e) Random-sized, PBC, without HC; (f) Regular, PBC, HC, with channels removal.

where μ is the fluid viscosity, and l_i and d_i are the length and diameter of channel i, respectively.

To obtain the pressure and flow fields, given respectively by the values of p_j and q_i, the mass conservation and the momentum equations must be written for all chambers and channels, resulting in a system of linear equations.[18,22] This leads to a sparse symmetric positive definite matrix, having a maximum number of seven nonzero entries per row that was solved using an appropriate solver (NAG^{TM} routine F04MCF).

Residence time distribution

From a global point of view, an important insight on the network hydrodynamics may be gained by analyzing the

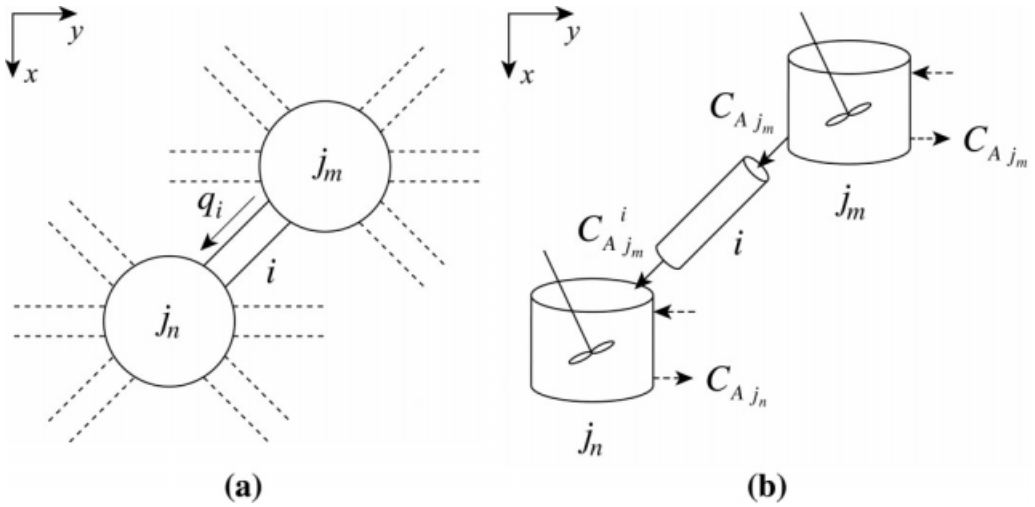

Figure 3. Chemical reaction model: (a) network branch; (b) analogy with a cascade of continuous-flow reactors.

Residence Time Distribution (RTD) function, $E(t)$. In this work, the RTD concerns the age distribution of the fluid elements that are in the effluent stream and is a characteristic of the mixing occurring within the network (macromixing), neglecting, however, detailed information on different mixing levels (micromixing). Even though not all RTDs are unique to a particular network, and markedly different network geometries can display similar RTDs, the RTD exhibited by a network provides important information for the characterization of the network.

In the NETmix® model, mixing between different streams occurs only in the chambers, thus defining two distinct zones: a perfectly mixed volume associated to the chambers and a segregated volume associated to the channels. A measure of the importance of each zone is given by the segregation parameter,

$$\alpha = \frac{V_{\text{channels}}}{V_{\text{network}}} \tag{5}$$

defined as the ratio between the volume associated to the channels, V_{channels}, and the total network volume, V_{network}.

Regular Networks with PBC. For the particular case of regular networks with PBC, an analytic solution for the dimensionless RTD function can be derived. Assuming that the total volumetric flow rate in the network, q_T, is constant and equally divided between all inlet channels, the hydrodynamics of a regular network with PBC is analogue to an alternate sequence of n_x piston flow channels and perfectly mixed chambers finishing with one piston flow channel at the exit. The respective dimensionless RTD function, $E(\theta)$, is given by[51]

$$E(\theta) = \frac{n_x}{(1-\alpha)(n_x-1)!}\left(\frac{n_x(\theta-\alpha)}{1-\alpha}\right)^{n_x-1} e^{-\frac{n_x(\theta-\alpha)}{1-\alpha}} H(\theta-\alpha) \tag{6}$$

where $\theta = t/\tau$ is the dimensionless residence time, $\tau = V_{\text{network}}/q_T$ is the mean residence time, and $H(t)$ is the Heaviside function.

Thus, for the particular case of regular networks with PBC, the network RTD function may be directly estimated using the network geometric parameters and the volumetric flow rate.

On the other hand, for other network types, regular or random-sized, analytic solutions for the RTD functions cannot be obtained. Nevertheless, for the case of regular networks with NPBC and high n_y values, Eq. 6 is a good approximation of the exact RTD function.

Chemical reaction

The NETmix® model uses a networks-of-zones model formulation based on the mixing behavior of two different ideal continuous-flow reactors, each associated to one type of network elements:

- channels behave as plug-flow reactors (PFR), zones of total segregation;
- chambers behave as perfectly mixed continuous stirred tank reactors (CSTR), zones of complete mixing.

A representation of the analogy between the network model and the equivalent CSTR and PFR series is shown in Figure 3.

Combining the network flow field results with the well-known conservation equations for each CSTR and PFR, a chemical reaction model, coupling macromixing and micromixing can be implemented. Three reaction schemes, described next, were studied in this work: a first order, second order, and a consecutive and competitive second-order reaction.

Case studies

First Order Reaction. Consider a network branch, shown in Figure 3a, and the schematic representation of its analogue cascade of continuous-flow reactors, shown in Figure 3b, and assume that the fluid in channel i flows towards chamber j_n. For a first-order reaction, $A \xrightarrow{k_1} B$, with rate law given by $-r_A = k_1 C_A$, where k_1 is the reaction rate constant and C_A is the concentration of reactant A; from the reactant molar balance in a CSTR, it results

$$C_{Aj_n} - \frac{\sum_i \left[\left(1 - I_{i,j_n}\right) q_i C^i_{Aj_m}\right] - k_1 V_{j_n} C_{Aj_n}}{\sum_i \left(I_{i,j_n} q_i\right)} = 0 \tag{7}$$

where q_i is the flow rate in channel i, V_{j_n} is the volume of chamber j_n, and I_{i,j_n}, indicating the flow direction, it is set to 0 if the stream in channel i is an inlet stream to chamber j_n, and it is set to 1 otherwise. $C^i_{\mathrm{A}j_\mathrm{m}}$ is the concentration at the exit of channel i, entering chamber j_n, and it can be obtained from the reactant molar balance in a PFR,

$$C^i_{\mathrm{A}j_\mathrm{m}} = e^{-k_1\frac{V_i}{q_i}} C_{\mathrm{A}j_\mathrm{m}} \tag{8}$$

where $C_{\mathrm{A}j_\mathrm{m}}$ is the concentration in chamber j_m, and V_i is the volume of channel i.

Combining Eqs. 7 and 8 for all chambers and channels, results in a linear system of n_{chambers} equations to be solved for the concentration of reactant A in each network chamber.

Second order Reaction. For a second-order reaction, $\mathrm{A} + \mathrm{B} \xrightarrow{k_2} \mathrm{R}$, with rate law given by $-r_\mathrm{A} = k_2 C_\mathrm{A} C_\mathrm{B}$, where k_2 is reaction rate constant, the concentration of reactants A and B in chamber j_n, $C_{\mathrm{A}j_\mathrm{n}}$, and $C_{\mathrm{B}j_\mathrm{n}}$, respectively, can be obtained by

$$C_{\mathrm{A}j_\mathrm{n}} - \frac{\sum_i \left[\left(1 - I_{i,jn}\right) q_i C^i_{\mathrm{A}j_\mathrm{m}}\right] - k_2 V_{j_\mathrm{n}} C_{\mathrm{A}j_\mathrm{n}} C_{\mathrm{B}j_\mathrm{n}}}{\sum_i \left(I_{i,jn} q_i\right)} = 0 \tag{9}$$

$$C_{\mathrm{B}j_\mathrm{n}} - C_{\mathrm{A}j_\mathrm{n}} - \frac{\sum_i \left[\left(1 - I_{i,jn}\right) q_i C^i_{\mathrm{B}j_\mathrm{m}}\right] - \sum_i \left[\left(1 - I_{i,jn}\right) q_i C^i_{\mathrm{A}j_\mathrm{m}}\right]}{\sum_i \left(I_{i,jn} q_i\right)} = 0 \tag{10}$$

where $C^i_{\mathrm{A}j_\mathrm{m}}$ and $C^i_{\mathrm{B}j_\mathrm{m}}$ are the concentrations at the outlet of channel i, entering chamber j_n, and they are related to the concentrations in chamber j_m, $C_{\mathrm{A}j_\mathrm{m}}$, and $C_{\mathrm{B}j_\mathrm{m}}$, by

$$\begin{cases} C^i_{\mathrm{A}j_\mathrm{m}} = \dfrac{C_{\mathrm{A}j_\mathrm{m}}}{1 - k_2 \frac{V_i}{q_i} C_{\mathrm{A}j_\mathrm{m}}} & \text{if} \quad C_{\mathrm{A}j_\mathrm{m}} = C_{\mathrm{B}j_\mathrm{m}} \\ C^i_{\mathrm{A}j_\mathrm{m}} = \dfrac{\frac{C_{\mathrm{A}j_\mathrm{m}}\left(C_{\mathrm{B}j_\mathrm{m}} - C_{\mathrm{A}j_\mathrm{m}}\right)}{C_{\mathrm{B}j_\mathrm{m}}} e^{-k_2 \frac{V_i}{q_i}\left(C_{\mathrm{B}j_\mathrm{m}} - C_{\mathrm{A}j_\mathrm{m}}\right)}}{1 - \frac{C_{\mathrm{A}j_\mathrm{m}}}{C_{\mathrm{B}j_\mathrm{m}}} e^{-k_2 \frac{V_i}{q_i}\left(C_{\mathrm{B}j_\mathrm{m}} - C_{\mathrm{A}j_\mathrm{m}}\right)}} & \text{if} \quad C_{\mathrm{A}j_\mathrm{m}} \neq C_{\mathrm{B}j_\mathrm{m}} \end{cases} \tag{11}$$

and

$$C^i_{\mathrm{B}j_\mathrm{m}} = C_{\mathrm{B}j_\mathrm{m}} - \left(C_{\mathrm{A}j_\mathrm{m}} - C^i_{\mathrm{A}j_\mathrm{m}}\right) \tag{12}$$

Combining Eqs. 9–12 for all chambers and channels, results in a nonlinear system of $2n_{\mathrm{chambers}}$ equations to be solved for the concentrations of reactants A and B.

Consecutive Competitive Second-Order Reactions. For the case of the consecutive competitive second-order reactions,

$$\begin{array}{l} \mathrm{A} + \mathrm{B} \xrightarrow{k_1} \mathrm{R} \\ \mathrm{B} + \mathrm{R} \xrightarrow{k_2} \mathrm{S} \end{array} \quad \begin{cases} -r_\mathrm{A} = k_1 C_\mathrm{A} C_\mathrm{B} \\ r_\mathrm{S} = k_2 C_\mathrm{B} C_\mathrm{R} \end{cases} \tag{13}$$

where k_1 and k_2 are the corresponding reaction rate constants. The concentrations of reactants A and B, $C_{\mathrm{A}j_\mathrm{n}}$ and $C_{\mathrm{B}j_\mathrm{n}}$, and of the intermediate product R in chamber j_n, $C_{\mathrm{R}j_\mathrm{n}}$, can be calculated from

$$C_{\mathrm{A}j_\mathrm{n}} - \frac{\sum_i \left[\left(1 - I_{i,j_\mathrm{n}}\right) q_i C^i_{\mathrm{A}j_\mathrm{m}}\right] - k_1 V_{j_\mathrm{n}} C_{\mathrm{A}j_\mathrm{n}} C_{\mathrm{B}j_\mathrm{n}}}{\sum_i \left(I_{i,j_\mathrm{n}} q_i\right)} = 0 \tag{14}$$

$$C_{\mathrm{B}j_\mathrm{n}} - \frac{\sum_i \left[\left(1 - I_{i,j_\mathrm{n}}\right) q_i C^i_{\mathrm{B}j_\mathrm{m}}\right] - k_1 V_{j_\mathrm{n}} C_{\mathrm{A}j_\mathrm{n}} C_{\mathrm{B}j_\mathrm{n}} - k_2 V_{j_\mathrm{n}} C_{\mathrm{B}j_\mathrm{n}} C_{\mathrm{R}j_\mathrm{n}}}{\sum_i \left(I_{i,j_\mathrm{n}} q_i\right)} = 0 \tag{15}$$

$$C_{\mathrm{R}j_\mathrm{n}} - \frac{\sum_i \left[\left(1 - I_{i,j_\mathrm{n}}\right) q_i C^i_{\mathrm{R}j_\mathrm{m}}\right] + k_1 V_{j_\mathrm{n}} C_{\mathrm{A}j_\mathrm{n}} C_{\mathrm{B}j_\mathrm{n}} - k_2 V_{j_\mathrm{n}} C_{\mathrm{B}j_\mathrm{n}} C_{\mathrm{R}j_\mathrm{n}}}{\sum_i \left(I_{i,j_\mathrm{n}} q_i\right)} = 0 \tag{16}$$

where $C^i_{\mathrm{A}j_\mathrm{m}}$, $C^i_{\mathrm{B}j_\mathrm{m}}$, and $C^i_{\mathrm{R}j_\mathrm{m}}$ are the concentrations at the outlet of channel i, entering chamber j_n.

In this case, the molar conservation equations for the network channel i do not present an analytic solution, and thus $C^i_{\mathrm{A}j_\mathrm{m}}$, $C^i_{\mathrm{B}j_\mathrm{m}}$, and $C^i_{\mathrm{A}j_\mathrm{m}}$ are obtained by solving for $V = V_i$ the respective set of first-order nonlinear of ordinary differential equations (ODEs).

$$q_i \frac{dC_\mathrm{A}}{dV} + k_1 C_\mathrm{A} C_\mathrm{B} = 0 \tag{17}$$

$$q_i \frac{dC_\mathrm{B}}{dV} + k_1 C_\mathrm{A} C_\mathrm{B} + k_2 C_\mathrm{B} C_\mathrm{R} = 0 \tag{18}$$

$$q_i \frac{dC_\mathrm{R}}{dV} - k_1 C_\mathrm{A} C_\mathrm{B} + k_2 C_\mathrm{B} C_\mathrm{R} = 0 \tag{19}$$

with boundary conditions $C_\mathrm{A}(0) = C_{\mathrm{B}j_\mathrm{m}}$, $C_\mathrm{B}(0) = C_{\mathrm{B}_{j_\mathrm{m}}}$, and $C_\mathrm{R}(0) = C_{\mathrm{R}j_\mathrm{m}}$, where $C_{\mathrm{A}j_\mathrm{m}}$, $C_{\mathrm{B}j_\mathrm{m}}$, and $C_{\mathrm{R}j_\mathrm{m}}$ are the concentrations in chamber j_m.

Solving the system of ODEs given by Eqs. 17–19, and replacing in Eqs. 14–16 for all network chambers and channels results in a nonlinear system of $3n_{\mathrm{chambers}}$ equations, to be solved for the concentrations of reactants A, B, and R in each network chamber.

Numerical implementation

The chemical reaction model was implemented in a software package written in Fortran 90 and compiled with Absoft™ Pro Fortran for Mac™ OS X v8.0. It has a sequential structure, as the chemical reaction simulation is based on data obtained from the network construction and the hydrodynamic models. Different numerical strategies must be considered depending on the reaction scheme. Figure 4 shows a diagram of the chemical reaction simulator and its relationship with the network generator and flow simulator.

For a first order reaction, for a given constant volumetric flow rate, q_T, the required input parameters to define the problem are just the reaction rate constant, k_1, and the feeding concentration distribution of reactant A, that is, its concentration at each inlet channel.

The resulting n_{chambers} linear equation system may be formulated as a band system of linear equations, and solved

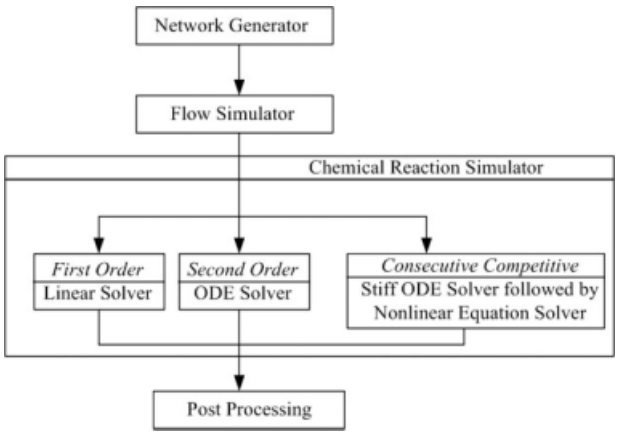

Figure 4. Fluxogram of the chemical reaction model simulator.

using an appropriate solver (NAG™ routine F07BEF, preceded by a call of NAG™ routine F07BDF to compute the LU factorization of the coefficient matrix).

In the case of a second-order reaction, additional degrees of freedom are introduced. Besides the volumetric flow rate, q_T, the reaction rate constant, k_2, and the feeding concentration distributions of both A and B, it is further required to set independently the inlet channels associated to each reactant, that is, the reactants injection scheme. The resulting $2n_{chambers}$ nonlinear equation system was solved using IMSL™ routine DNEQNF, based on the MINPACK subroutine HYBRD1, which uses a modified Powell hybrid algorithm. The stopping criterion for the solution to be accepted was set for a relative error between two successive approximations less than 10^{-6}.

For consecutive competitive second-order reactions, besides the two reaction rate constants, k_1 and k_2, the required input parameters are similar to those for a second-order reaction. The $3n_{chambers}$ nonlinear equation system was also solved using IMSL™ routine DNEQNF. The system of first-order nonlinear ODEs was solved using IMSL™ routine DIVPAG, which solves an initial-value problem for ordinary differential equations using Gear's BDF method, appropriate for solving stiff ODE problems.

All simulations were performed on a Apple PowerMac. In terms of computation time, for the networks considered in this work, the network generation and the calculation of the flow field took on average 15 and 30 min, respectively. The determination of the concentration profiles depends on the chemical reaction scheme considered. For first-order, second-order, and consecutive competitive second-order reaction schemes, the average computation times were of the order of 15, 30, and 240 min, respectively, with small variations depending on the characteristics of the network, in particular its elements size distribution.

Simulations and Results

The NETmix® model is capable of describing various mixing states, by considering appropriate network input parameters and network types. All simulations were performed for regular networks with PBC and without HC. However, the purpose of this work is not to present a parametric systematic study of the effect of the model parameters on the model predictions, but to show that the model is capable of coupling micromixing with macromixing and simultaneously retain the distinction between both. Other parameters may be calculated based on the NETmix model, such as the longitudinal and transverse dispersion coefficients. The first parameter can be estimated from the dimensionless RTD functions obtained by the model and matching the second statistical moment of the response with the predictions of the dispersion model.[4] The transverse diffusion coefficient can be estimated comparing the concentration profiles predicted by the NETmix model and the dispersion model for a point perturbation.[52]

Macromixing

Macromixing is determined from the reactor hydrodynamics and is commonly assessed from the RTD. For regular networks, the theoretical RTD function given by Eq. 6, depends directly on just two parameters, the number of rows, n_x, and the segregation parameter, α, which were studied separately.

Plots of the RTD functions for regular networks with $n_x = 10$ and $n_x = 50$, respectively, and segregation parameter values ranging from $\alpha = 0.010$ to $\alpha = 0.750$ are shown in Figures 5a,b. For a fixed number of rows, the behavior of the system approaches that of the PFR as the segregation parameter tends to unity. Such result is easily understood recalling that as the chambers volume is reduced, the network structure tends to a battery of plug-flow reactors in series, equivalent to a single plug-flow reactor with the same mean residence time.

Figures 5c,d, show plots of the RTD functions for regular networks for $\alpha = 0.100$ and $\alpha = 0.500$, respectively, and number of rows ranging from $n_x = 5$ to $n_x = 100$. For a given segregation parameter, as the number of rows increases the system approaches a PFR, as expected from the network structure similarity with the tanks-in-series model (TISM).[4] Simulations have further shown to exist no significant changes on $E(\theta)$ for values of α lower than 0.010.

Figure 6 compares the RTD functions for four networks with different values of n_x and α listed in Table 1, showing that similar RTDs can be obtained for different network geometries.

A common method of characterizing the RTD in flow systems is by comparing the moments of each distribution, instead of comparing the whole distribution.[53] The first three moments are usually sufficient for a reasonable characterization of a RTD, although rigorously all moments would need to be compared.

The first moment is the dimensionless mean residence time, defined as

$$\theta_m = \int_0^\infty E(\theta)d\theta \tag{20}$$

and using the regular network $E(\theta)$ (Eq. 6), it can be shown that $\theta_m = 1$. The second centered moment is taken about the mean and is denoted as the variance. The magnitude of the variance represents the square of the distribution spread and

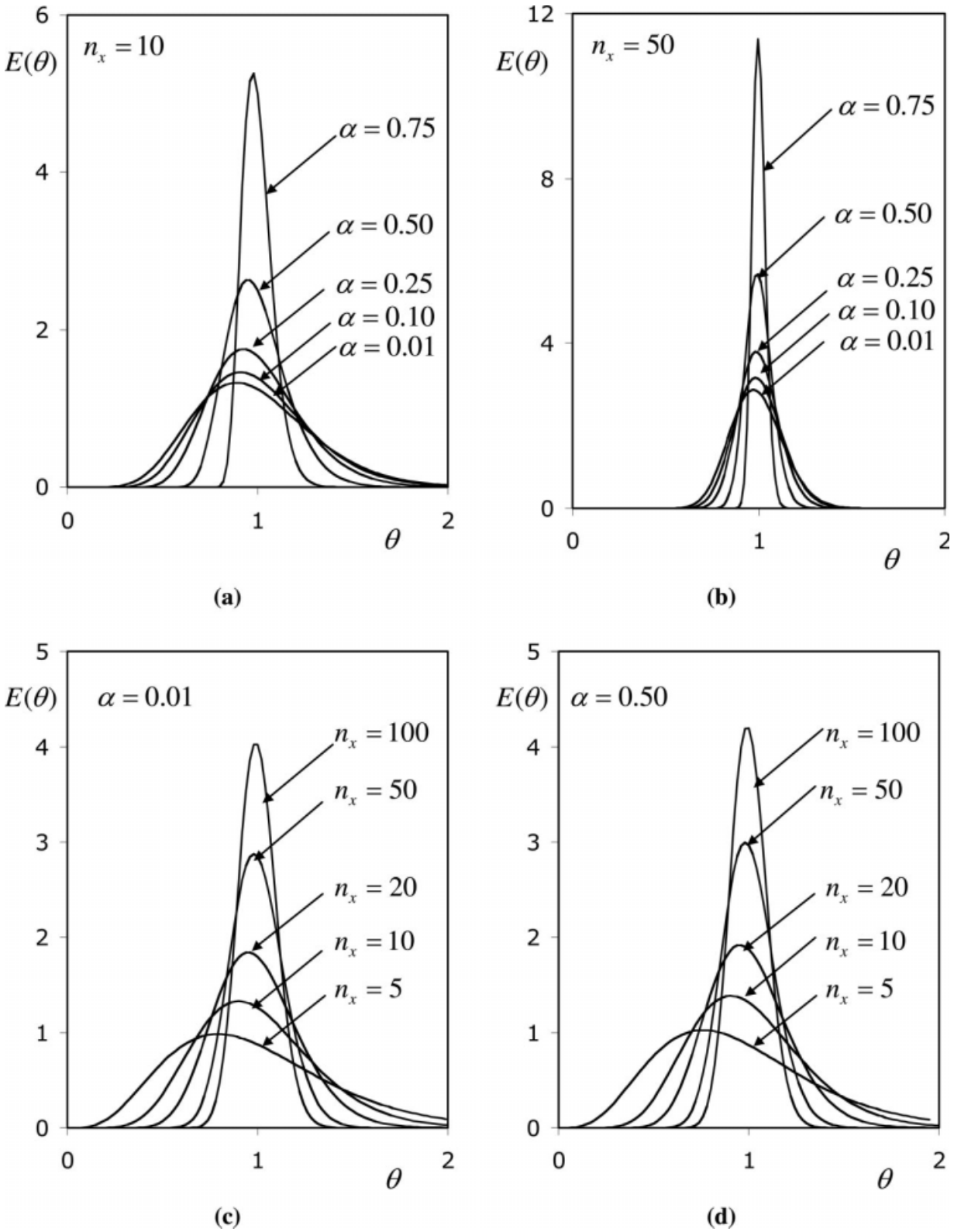

Figure 5. RTDs for regular networks for: (a) $n_x = 10$; (b) $n_x = 50$; (c) $\alpha = 0.010$; (d) $\alpha = 0.500$.

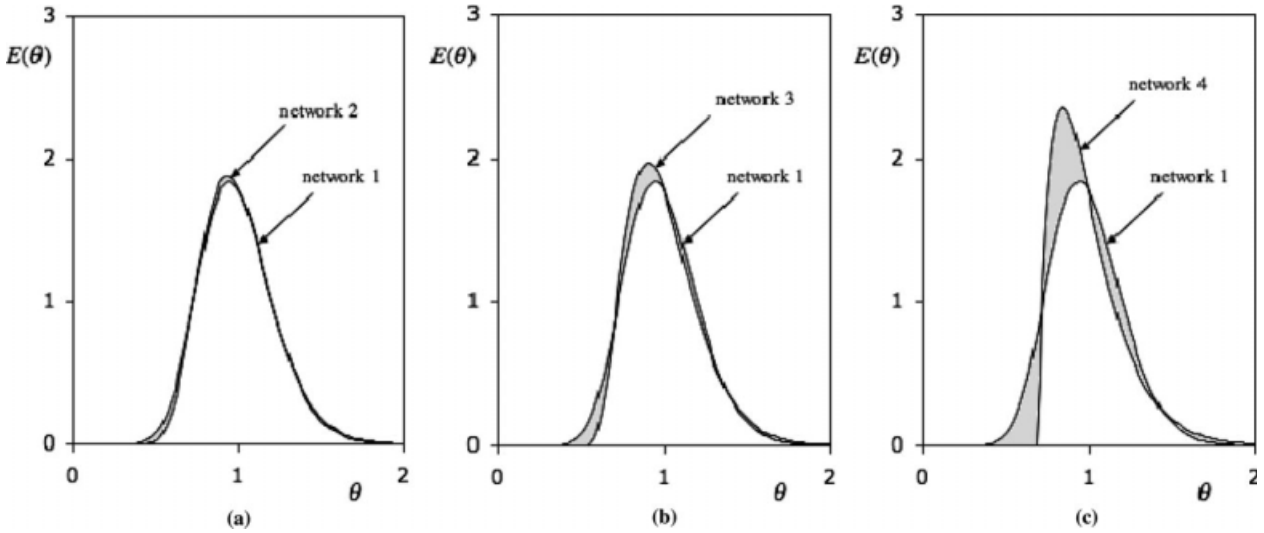

Figure 6. Comparison of RTDs for different networks.

the greater the value of this moment, the greater the spread of the RTD. For a regular network, an analytical expression can also be obtained.

$$\sigma^2 = \int_0^\infty (1-\theta)^2 E(\theta) d\theta = \frac{(1-\alpha)^2}{n_x} \tag{21}$$

This result shows that it is possible to design regular networks having different values of n_x and α, with matching first and second moments.

The third centered moment is also taken about the mean and is related to the RTD skewness.

$$s^3 = \frac{1}{\sigma^{3/2}} \int_0^\infty (1-1/\theta)^3 E(\theta) d\theta \tag{22}$$

The magnitude of this moment measures the extent to which the distribution is skewed in one direction or another in reference to the mean. No analytical solution was obtained for s^3 and a numerical quadrature was used to approximate the integral in Eq. 22.

The four networks listed in Table 1 all have the same variance, σ^2, but different values of s^3. Although it is clear that s^3 increases as the difference between RTD's increases, it is not possible to quantify how similar they really are only based on these values.

Another methodology used for the characterization of RTDs is based on the deterministic role of macromixing in the yield of first-order reactions regardless of micromixing effects.[54] For a first-order reaction, the yield is defined by

$$X_A = \frac{C_A^{in} - C_A^{exit}}{C_A^{in}} \tag{23}$$

where C_A^{in} and C_A^{exit} are the average network inlet and exit outlet concentrations of reactant A. The extent of micromixing does not affect the rate of change of yield and so the RTD is sufficient to calculate the yield in any type of reactor. In this way, two different regular networks may be assumed to have similar macromixing if both RTD functions have similar first and second moments and both networks lead to similar yields for a first-order reaction under the same reaction conditions. Using the segregation model,[54,55] the mean reaction yield is given by

$$X_A = \int_0^\infty X_A(t) E(t) dt \tag{24}$$

where $X_A(t) = 1 - e^{-k_1 t}$ is the batch reactor yield.

For a regular network, assuming a uniform concentration of reactant A at all inlet channels, it can be shown that

$$X_A = 1 - \left[\frac{e^{-\alpha Da}}{\left(k_1 \left(\frac{1-\alpha}{n_x}\right)(\tau+1)\right)^{n_x}} + \frac{(-1)^{n_x-1} e^{-\alpha Da}}{\left(k_1 \left(\frac{1-\alpha}{n_x}\right)(\tau+1)\right)(n_x-1)!} \Gamma(n_x, -\alpha Da) \right] \tag{25}$$

Table 1. Parameter List and Macromixing Result Data for Different Regular Networks

	n_x	α	θ_m	σ^2	s^3	X_A (%)	$\Delta E_{1,j}$ (%)
Network 1	20	0.010	1	4.900×10^{-2}	4.85×10^{-3}	62.33	0.00
Network 2	10	0.300	1	4.900×10^{-2}	6.86×10^{-3}	62.34	4.98
Network 3	5	0.505	1	4.900×10^{-2}	9.70×10^{-3}	62.36	12.5
Network 4	2	0.687	1	4.901×10^{-2}	1.53×10^{-2}	62.39	30.2

where $\Gamma(k,x)$ is the incomplete gamma function and $Da = k_1\tau$ is the Damköhler number. For large n_x values, it can be shown that the mean yield reduces to

$$X_A = 1 - \left(Da\left(\frac{1-\alpha}{n_x}\right) + 1 \right)^{-n_x} e^{-\alpha Da} \tag{26}$$

Yield values for $Da = 1$ are listed in Table 1 for the four regular networks, showing that although a slight increase in yield is observed as the difference in RTDs increases, again these results do not allow quantifying these differences.

To quantify the differences in the RTD functions another methodology is here presented. Assuming that the first and second moments of two RTD functions, $E_i(\theta)$ and $E_j(\theta)$, are equal, an heuristic evaluation criteria may be obtained by overlapping both curves and determining the area of the nonintersecting regions (shaded regions in Figure 6) as

$$\Delta E_{i,j} = \frac{\int_0^\infty \left| E_i(\theta) - E_j(\theta) \right| d\theta}{\int_0^\infty E_i(\theta) d\theta} \tag{27}$$

The nonintersecting areas for the four RTD functions relative to network 1, $\Delta E_{1,j}$, are listed in Table 1. Contrary to the previous criteria, the heuristic evaluation criterion of Eq. 27 shows responsiveness and correlation with the degree of resemblance between the different RTDs. Thus it seems acceptable to assume that two networks with the same $\Delta E_{i,j}$ have similar RTDs, that is, similar macromixing behavior.

Micromixing and chemical reaction

Micromixing is here directly assessed from chemical reaction simulations with a twofold importance. First, with the purpose of validating the NETmix® model numerical implementation, using first-order and second-order reactions, are compared in the next two subsections, with case studies for which chemical reaction results are known from previous relevant works. Second, the validated NETmix® model is used to study the effect of the network input parameters on the reaction selectivity of consecutive-competitive second-order reactions.

First Order Reaction. For a first-order reaction, micromixing has no effect on the reactor performance. Therefore, the yield is predicted exactly by the segregation model and knowledge of the degree of micromixing is not required. This well known result is next used to query the numerical implementation.

Two particular regular networks based on the networks 1 and 2 of Table 1 were constructed with the required input parameters listed in Table 2. These parameters were obtained imposing that the network volumes do not differ more 0.5%. Simulations were carried out for a first-order reaction with reaction rate constant $k_1 = 1.0\ s^{-1}$, for $Da = 1$ and with a constant feed concentration distribution of reactant A equal to $C_A^{inlet} = 1.0\ mol\ m^{-3}$.

The yield values obtained with the chemical reaction simulator exactly matched the results obtained with the segregation model listed in Table 1, thus validating the NETmix® model simulations.

Table 2. Input Parameters for Networks 1 and 2

	Network 1	Network 2
n_x	20	10
n_y	16	173
d (mm)	1.500	1.500
D (mm)	9.064	4.617
L^o (mm)	10.00	10.00
ϕ	45°	45°
$V_{network}$ (cm^3)	126.0	126.3

Second Order Reaction. For reactions with order different than unity in the case where the reactants are premixed at the inlet, micromixing affects the yield: it decreases for orders greater than one and it increases for orders less than one.[56] This assertion is next compared with the simulations using the NETmix® model.

Using a second-order reaction scheme, the mean reaction yields for networks 1 and 2 were computed, considering equimolar inlet concentrations of reactants A and B and a reaction rate constant of $k_2 = 1.0\ m^3\ mol^{-1}\ s^{-1}$. For comparison purposes, both simulations were performed for $Da = k_2\tau\ C_A^{inlet} = 1$, with an initial concentration of reactant A of $C_A^{inlet} = 1.0\ mol\ m^{-3}$ and premixed injection scheme, with reactants A and B injected in every other feeding channel, maximizing the reactants feed distribution.

The mean reaction yields computed for networks 1 and 2 were 49.16% and 48.46%, respectively.

Even though the difference in the yields is small for the parameter values selected, the point to be emphasized is that there is a difference. Because micromixing decreases the yield for reaction orders greater than one, it can be directly inferred from these simulations that network 2 presents a higher degree of micromixing, that is, a higher effectiveness of mixing, than network 1.

This result constitutes evidence that the number of rows and the segregation parameter are not just macromixing parameters, but also micromixing parameters. Network 2 has a segregation parameter 30 times higher than network 1 (see Table 1), which contributes to a lower effectiveness of mixing, that is, higher mean reaction yield. On the other hand, network 2 has half the number of rows of network 1, contributing decisively in the opposite way, that is, to a higher effectiveness of mixing of network 2 and thus to a lower mean reaction yield. The overall degree of micromixing results thus from the simultaneous contribution of the number of rows and the segregation parameter. Both parameters work in the same manner, increasing micromixing as their values decrease. Furthermore, the agreement of the simulation results with theory highlights the good numerical implementation of the NETmix® model.

In the previous simulations, no relevance was given to the reactants injection scheme. Because mixing is akin to the spatial rearrangement of entities, different reactants injection schemes were used here, corresponding each to a different initial state of effectiveness of mixing.

Danckwerts[57] has shown, for second-order reactions, that if the purpose of mixing two reactants A and B is to enable them to react with one another, the highest rate of reaction is achieved when the inverse of the effectiveness of mixing is zero, that is, for the maximum mixedness condition. The

Table 3. List of Parameters for Each Segregated Injection Scheme

	C_A^{in} (mol m^{-3})	C_B^{in} (mol m^{-3})	n_{zones}	n_{zones}^B
Case 1a	2.000	2.000	2	1
Case 1b	2.000	2.000	4	2
Case 1c	2.000	2.000	8	4
Case 1d	2.000	2.000	16	8
Case 2a	1.143	8.000	3	1
Case 2b	1.333	4.000	5	2
Case 2c	1.333	4.000	7	3
Case 2d	1.600	2.667	11	5

agreement of the NETmix® model with this relevant result is next presented.

Using a second-order reaction, the mean reaction yield in network 1 was computed for different reactants injection schemes, corresponding each to a different degree of mixing in the reactants feed distribution, segregated injection schemes. All simulations were performed with $k_2 = 1.0$ m^3 mol^{-1} s^{-1} and $Da = 1$.

Table 3 lists the inlet concentrations of reactants A and B, according to each segregated injection scheme, as well as, a column with the number of injection zones, n_{zones}, and a column with the number reactant B injection zones, n_{zones}^B. Two different cases, denoted as Case 1 and Case 2, represented in Figure 7, were studied:

- In Case 1, the network inlet chambers are divided in a given even number of injection zones, n_{zones}, and reactants A and B are injected at the inlet channels of every other injection zone. Each injection zone comprises an equal number of inlet chambers and the number of injection zones where reactant B is injected is referred as number of reactant B injection zones, n_{zones}^B.
- In Case 2, reactant B is injected through the inlet channels of one or more separate reactant B injection zones, equally spaced, and reactant A is injected on the remaining injection zones. Each reactant B injection zone comprises a maximum of one or two inlet chambers. For each reactants injection scheme, the reactants concentrations, C_A^{in} and C_B^{in}, are adjusted to ensure the same average inlet concentrations of reactants A and B.

Figure 8 shows examples of the computed concentration field maps of reactant B and product R. The effect of the number of reactant B injection zones on the mean reaction yield, X_A, is shown in Figure 9, where the dashed curves represent the CSTR and the PFR limits using the premixed injection scheme. As expected, the average reaction yield increases with the increase in the number of reactant B injection zones, that is, as the initial state of effectiveness of mixing in the reactants is increased.

From Figure 9, it is also clear that, for low number of reactant B injection zones, Case 2 presents a more effective behavior in terms of the average reaction yield.

For a given number of reactant B injection zones there are, in both cases, $2n_{zones}^B$ contact fronts between A and B, but the reactants concentration gradients on these contact fronts is higher in Case 2 (Figure 8). This is the reason why

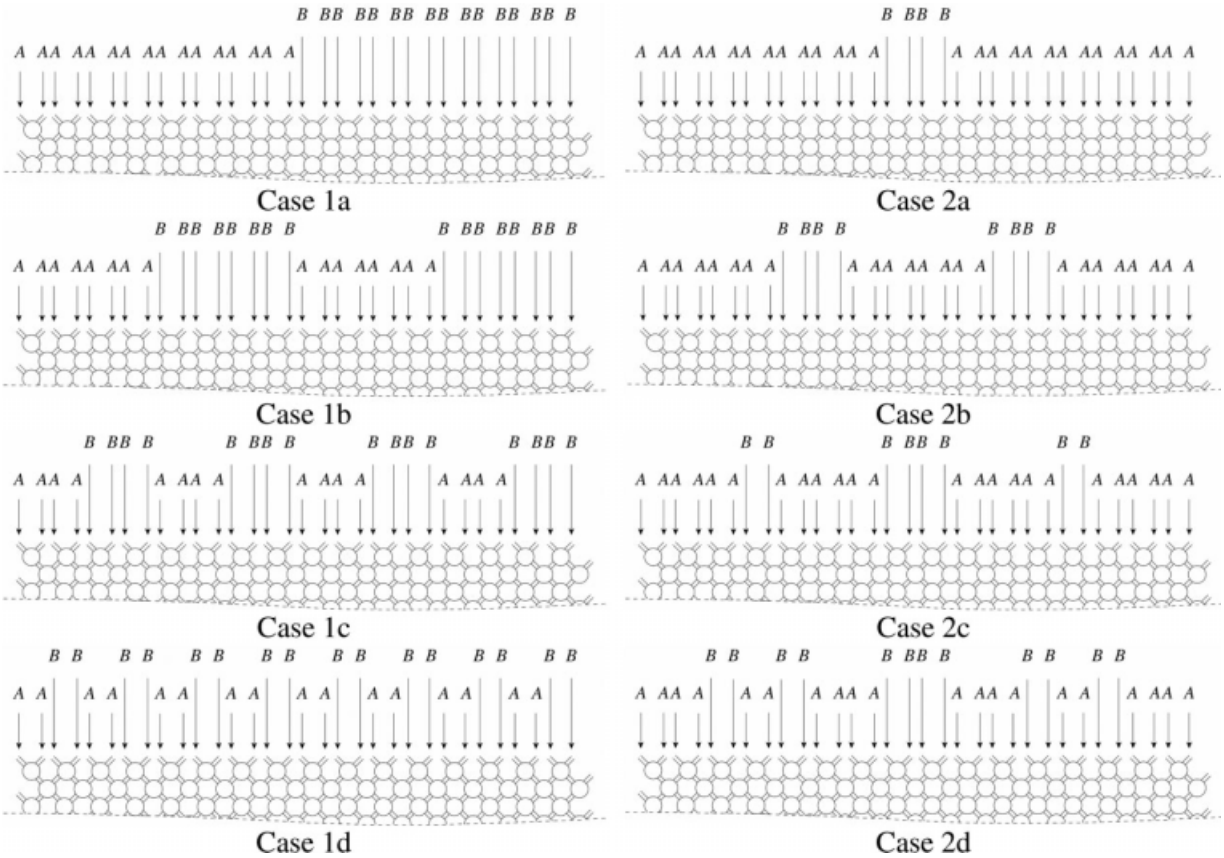

Figure 7. Representation of the different segregated injection schemes.

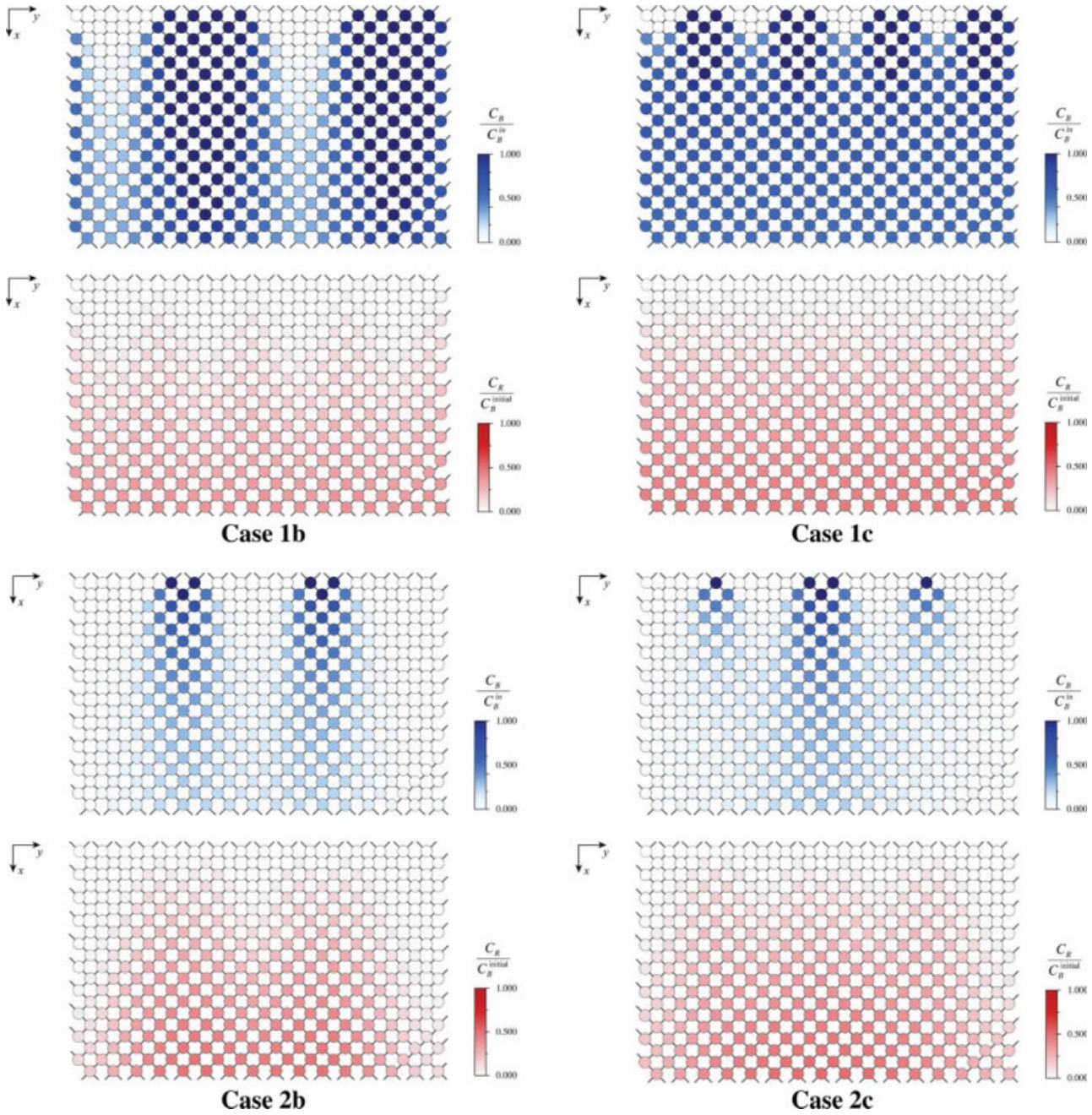

Figure 8. Concentration field maps of reactant B and product R in network 1 for various segregation injection schemes.

[Color figure can be viewed in the online issue, which is available at www.interscience.wiley.com.]

Case 2 presents higher values of X_A for $n_{zones}^B < 2$. However for $n_{zones}^B > 2$, Case 1 presents higher values of X_A, which may be due to better mixing between reactants. Both cases tend to the maximum limiting yield of 49.2%, which occurs for the premixed injection scheme, between the mean reaction yield of 38.2% for a CSTR and of 50.0%.

Consecutive Competitive Second-Order Reaction. The results for a second-order have shown that the reactants injection scheme strongly affects the average reaction yield, and therefore, it may be used as probe to study micromixing. Three parameters have been clearly identified to be related with micromixing: the number of rows, the segregation parameter, and the reactants injection scheme. The effect of all three parameters on micromixing is here further explored using the consecutive competitive second-order reactions scheme described by Eq. 13.

Multiple reactions offer a way to evaluate the predictions of models which aim to describe interactions between mixing and chemical reaction.[58] In the present reaction scheme, the selectivity in either product, R or S can be used to

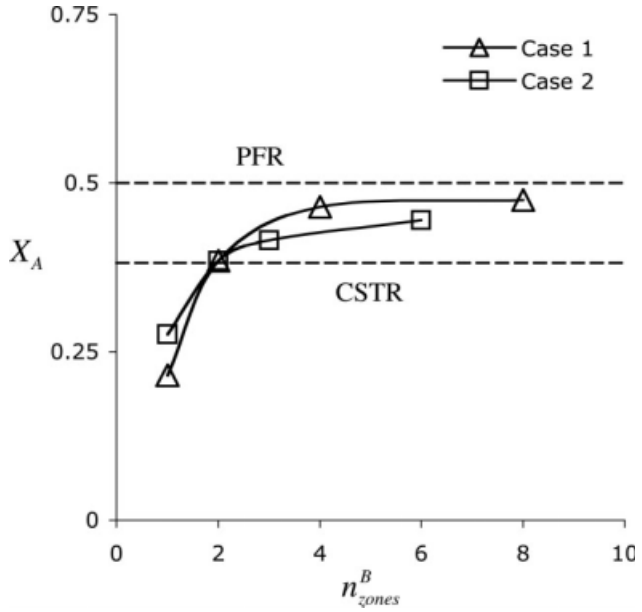

Figure 9. Average reaction yield vs. the number of reactant B injection zones.

express the product distribution. In this work, the resulting product distribution is expressed by the fraction of B present in S, that is, the selectivity in S, defined as[59]

$$X_S = \frac{2C_S^{exit}}{C_R^{exit} + 2C_S^{exit}} \tag{28}$$

where C_R^{exit} and C_S^{exit} are the average network exit concentration of products R and S, respectively.

Figure 10 shows the selectivity in S as a function of the Damköhler number, $Da = k_1\tau\ C_B^{in}$, for various regular networks with different values of n_x and α. All simulations results were obtained for $k_1 = 12{,}500\ m^3\ mol^{-1}\ s^{-1}$ and $k_2 = 1000\ m^3\ mol^{-1}\ s^{-1}$, using the premixed injection scheme, with reactants A and B injected at every other feeding channels, and considering equimolar initial concentrations of reactants A and B, with an inlet concentration of reactant A of $C_A^{in} = 1.0\ mol/m^{-3}$.

Because equimolar initial concentrations of reactants A and B are used, B becomes the limiting reactant, and thus the product distribution provides an assessment for micromixing. The dashed curves in these figures represent the limits for the CSTR and the PFR, obtained by classical kinetic methods.[53]

Figure 10 clearly shows that the segregation parameter has a strong impact on the selectivity in S, but X_S is always contained between the CSTR and the PFR limits. As the segregation parameter increases, X_S approaches the PFR curve, independently of the number of rows considered. This result is more noticeable in the lower range of Damköhler numbers, showing that for higher *Da* values increasingly smaller parts of the network are effectively used for reaction, up to the limit where reaction occurs only in the network inlet chambers, and thus all curves tend to overlap with the CSTR limit.

More, when comparing Figures 10a,b, for the same Damköhler number and similar segregation parameter, different selectivities in S are observed. These observations constitute further and final evidence of the impact of the number of rows and the segregation parameter on both macromixing and micromixing. However, contrary to the conclusions for macromixing, direct inference of the effect of the number of rows and the segregation parameter on micromixing is not possible because the macromixing conditions were not kept constant between the various simulated networks.

The above results and the results presented in the previous section have shown that using the premixed injection scheme, the CSTR limit for X_S cannot be reached.

Different segregated injection schemes, shown in Figure 11, were simulated using the same values for the kinetic constants and inlet concentrations as before. The curves of the selectivity in S against the Damköhler number are shown in Figure 12, where again the dashed curves represent the CSTR and the PFR limits, whereas the full dots curve represents X_S for the corresponding network using the premixed injection scheme.

Figure 12 shows that the use of segregated injection schemes, in general leads to higher X_S than the premixed

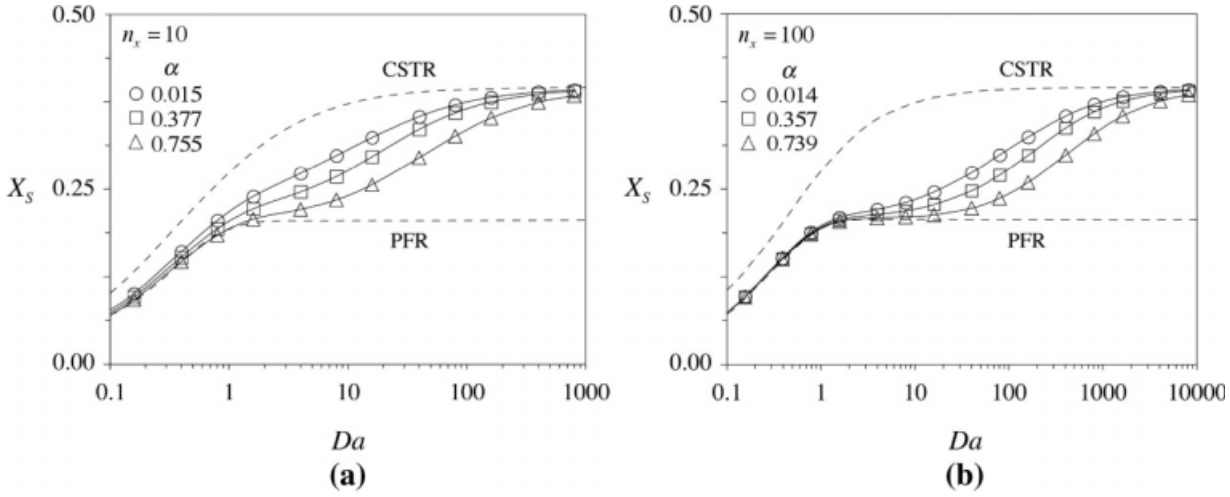

Figure 10. Selectivity in S vs. *Da* for different networks, using the premixed injection scheme.

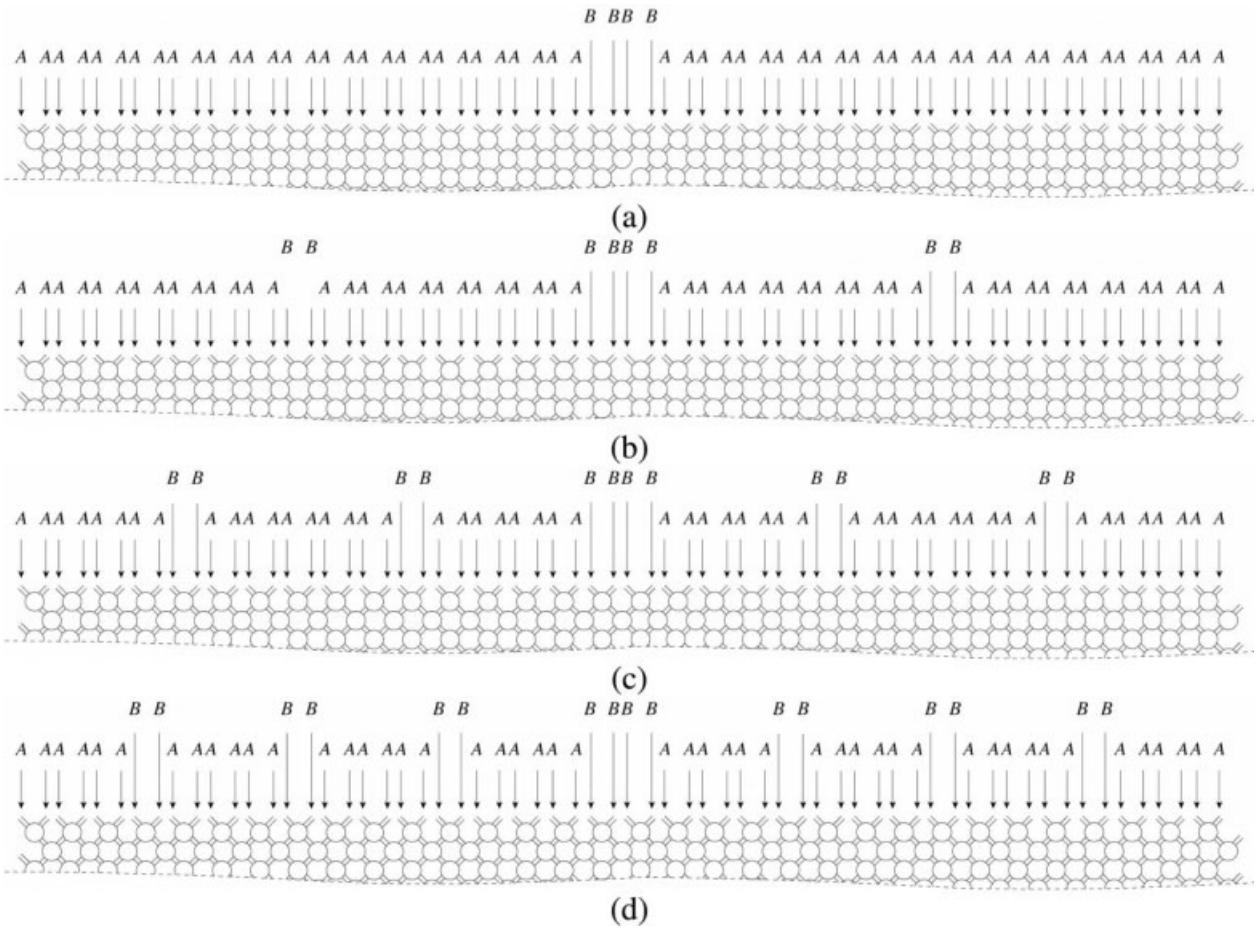

Figure 11. Segregated injection schemes used in the simulations shown in Figures 11 and 12.

injection scheme and also higher than CSTR limit. More, the increase in the number of reactant B injection zones results in a decrease in the selectivity in S, for the same Damköhler number. Figure 13 plots X_S vs. n^B_{zones}, for a particular network for $Da = 1$ and $Da = 10$, respectively, where once more, the dashed curves represent the CSTR and the PFR limits using the premixed injection scheme. These simulation results are in agreement with the well-known observation that the selectivity in S is, for similar consecutive competitive second-order reactions, reduced by promoting good

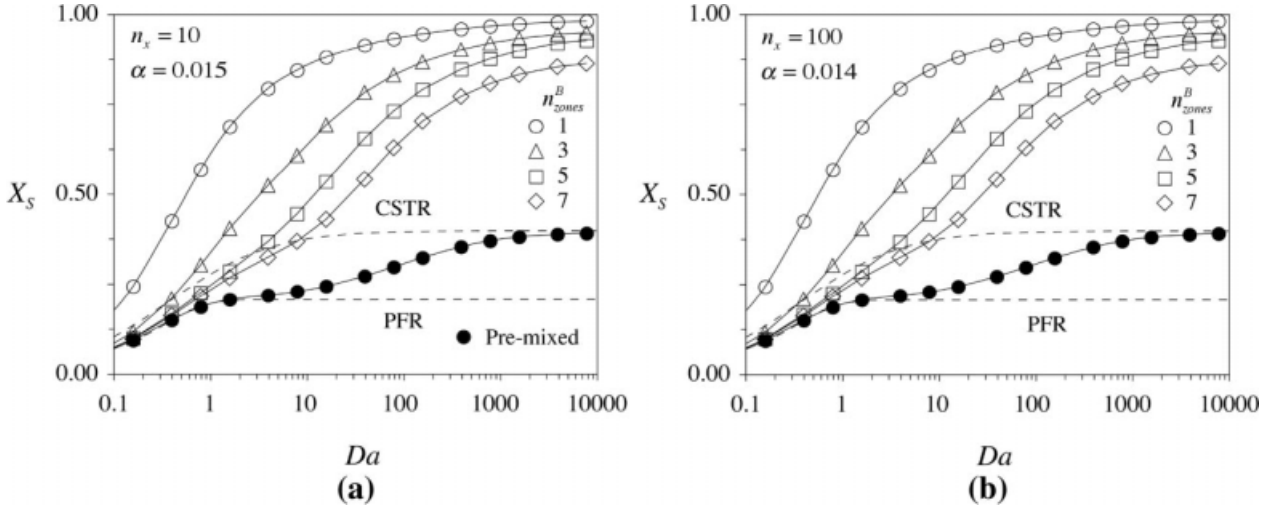

Figure 12. Selectivity in S vs. *Da* using different segregated injection schemes.

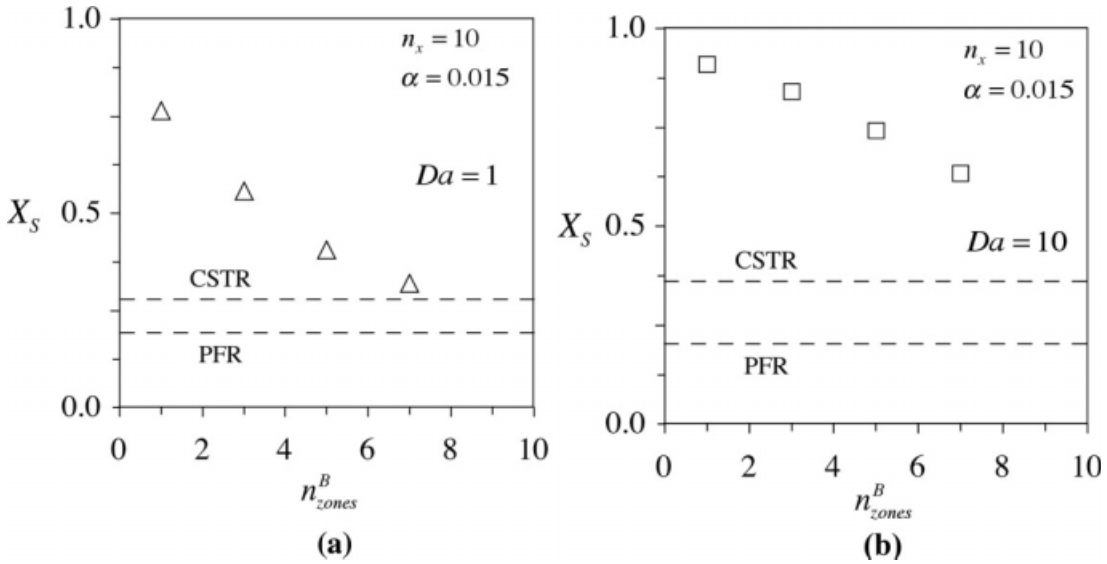

Figure 13. Plot of selectivity in S vs. the number of reactant B zones.

mixing between reactants A and B before significant reaction occurs, that is, by increasing the initial state of effectiveness of mixing of the reactants.[59,60]

For further insight into the use of segregated injections schemes, Figures 14 and 15 show the computed concentration field maps of reactant A and products

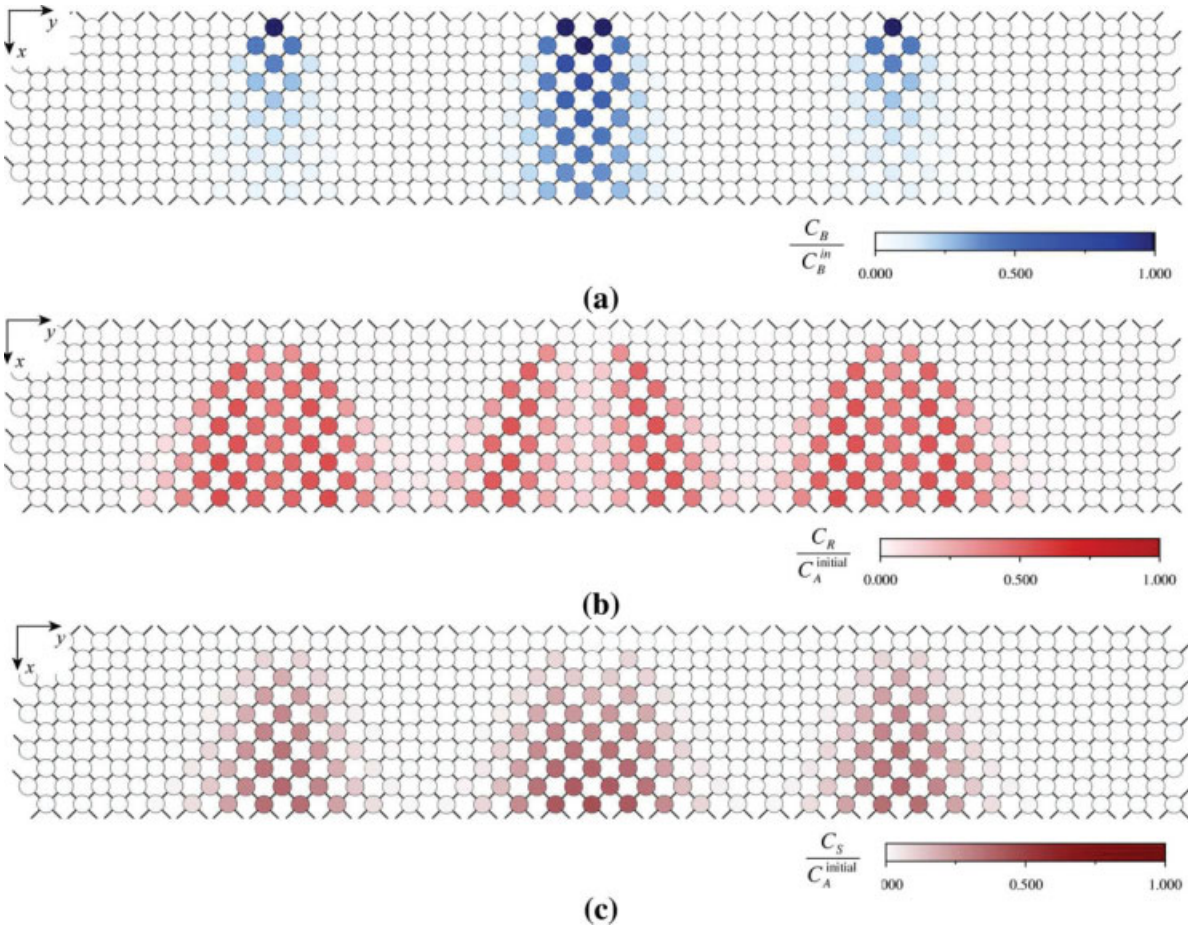

Figure 14. Concentration field maps of reactant A and products R and S for $n_x = 10$, $\alpha = 0.015$, $Da = 1$, and $n^B_{zones} = 3$.

[Color figure can be viewed in the online issue, which is available at www.interscience.wiley.com.]

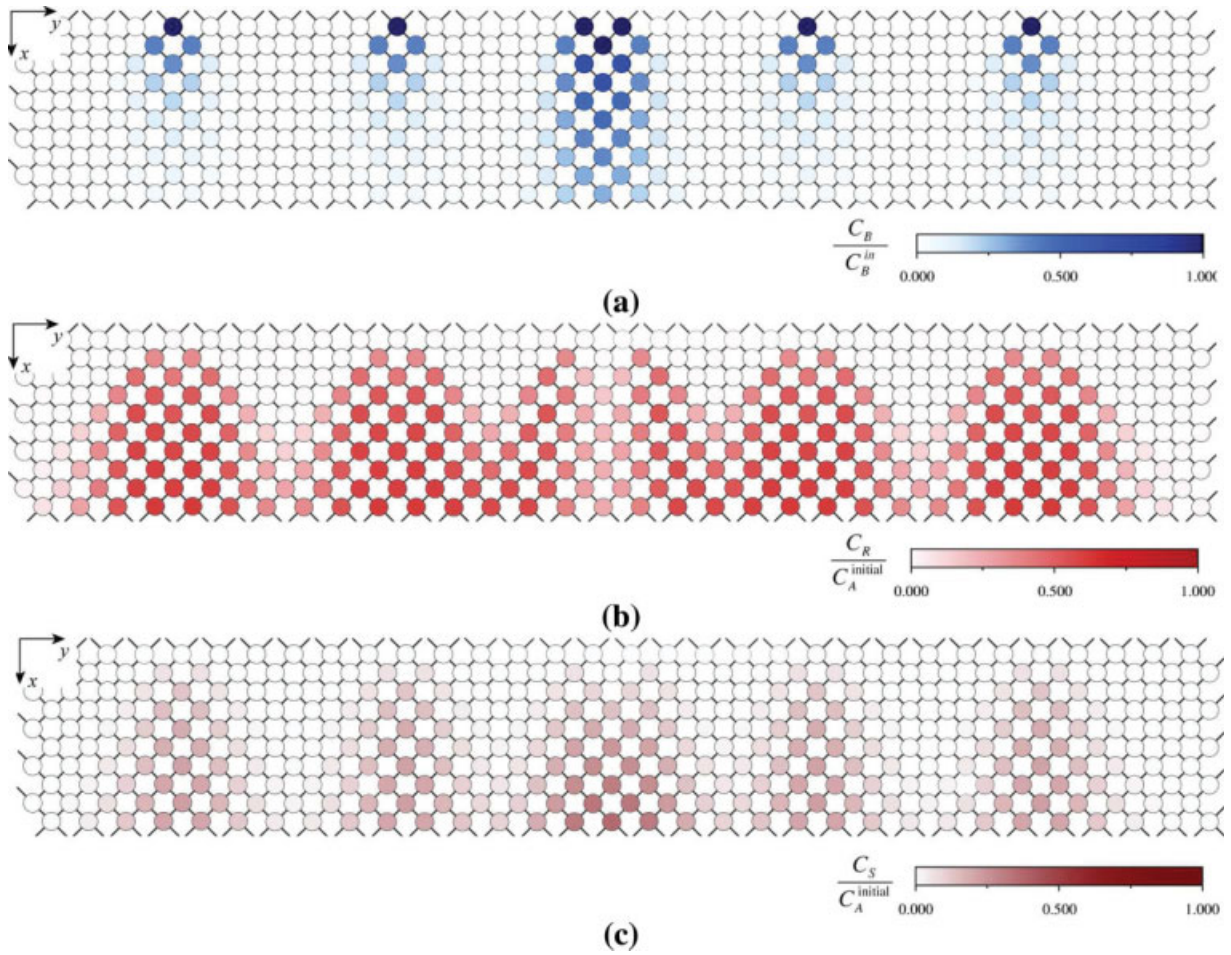

Figure 15. Concentration field maps of reactant A and products R and S for $n_x = 10$, $\alpha = 0.015$, $Da = 1$, and $n^{B}_{zones} = 5$.

[Color figure can be viewed in the online issue, which is available at www.interscience.wiley.com.]

R and S in a particular network for $Da = 1$ and n^{B}_{zones} variable.

The fact that reactants A and B are separately injected strongly affects products R and S distribution. Product R is mainly formed on the contact fronts between reactants A and B, with almost complete consumption of A. Conversely, product S is mainly formed between contact fronts were unreacted B promotes the consumption of R into S. The increase in the number of reactant B injection zones flattens the reactants concentration gradients, which causes reducing the excess of B present after consumption of A and preventing the formation of product S.

The NETmix® model is thus capable of describing with qualitative consistency the impact of the number of rows, segregation parameter and reactants injection scheme, as micromixing parameters, on the product distribution for consecutive competitive second-order reactions. Although different results are expected if the NETmix® model is 3D instead of 2D, from a qualitative point of view the results should be similar, as the main mechanisms of macro and micromixing are the same, and α is the relevant segregation parameter for this system.

Conclusions

Based on a network structure of unit cells, a new model for mixing has been developed. The unit cell of the NETmix® model consists of one chamber and three channels, modeled as a perfectly mixed continuous stirred tank reactor and plug-flow reactors, respectively.

The NETmix® model is a simple, practical simulation instrument, capable of straightforwardly be adjusted to specific situations, and it can serve as a basis for a diversity of calculations, and especially it gives a plausible description of chemical reaction under distinct macromixing and/or micromixing conditions.

Analysis of simulated RTDs lead to the development of a simple methodology to design regular networks having different design parameters but similar macromixing. The parameters identified to affect macromixing are: the number of rows and the segregation parameter.

Chemical reaction simulations were performed for three reaction schemes—first-order reaction, second-order reaction, and consecutive competitive second-order reactions—with the purpose of validating the model numerical implementation and studying the yield and selectivity dependency on micromixing.

For first-order reaction, the well-known result that the output is independent of micromixing was verified. Simulations for second-order reaction showed yield dependency on micromixing for network structures with indistinguishable yields for the first-order reaction, enabling the identification as micromixing parameters the number of rows and the segregation parameter. Second-order reaction simulations further revealed the reactants injection scheme to be the third micromixing related parameter.

Simulations for consecutive competitive second-order reactions showed strong product distribution dependency on the micromixing parameters. Under certain reactants injection schemes, the NETmix® structure leads to predicted selectivity values above the values obtained in classical type of reactors. The present model allows for a systematic investigation of macromixing and micromixing outcomes for different reaction schemes on different network structures, so that qualitative results obtained a priori can be used to design static mixers with a network structure with improved effects on both the yield and selectivity of reaction.

These findings have been the subject of an international patent application.[50] A prototype of the NETmix® static mixer was designed constructed and used for implementation of tracer and test reactions experiments for macro and micromixing studies.[48]

Acknowledgements

Financial support for this work was in part provided by national research grants FCT/PRAXIS/3/3.1/CEG/2565/95 and FCT/POCTI/EQU/34151/99 for which the authors are thankful. A.A. Martins and P.E. Laranjeira acknowledge their Ph.D. scholarships by FCT, PRAXIS XXI/BD/2631/93 and PRAXIS XXI/BD/21490/99, respectively.

Literature Cited

1. Villermaux J, Falk L. Recent advances in modelling micromixing and chemical reaction. *Revue de L' Nospace Institutefrançais du Pétrole*. 1996;51:205–213.
2. Zalc JM, Muzzio FJ. Parallel-competitive reactions in a Two-dimensional chaotic flow. *Chem Eng Sci*. 1999;54:1053–1069.
3. Sahimi M. *Flow and Transport in Porous Media and Fractured Rock. From Classical Methods to Modern Approaches*. Weinheim, Germany: Springer Verlag, 1995.
4. Fogler H. *Elements of Chemical Reaction Engineering*, 2nd ed. Upper Saddle River, NJ: Prentice-Hall, 1992.
5. Mehta RV, Tarbell JM. Four environment model of mixing and chemical reaction: I. model development. *AIChE J*. 1983;29:320–332.
6. Ioannidis MA, Chatzis I. Network modelling of pore structure and transport properties of porous media. *Chem Eng Sci*. 1993;48:951–972.
7. Thauvin F, Mohanty KK. Network modelling of non-darcy flow through porous media. *Transport Porous Med*. 1998;31:19–37.
8. Wang X, Thauvin F, Mohanty KK. Non-darcy flow through anisotropic porous media. *Chem Eng Sci*. 1999;54:1859–1869.
9. Berkowitz B, Ewing RP. Percolation theory and network modelling. *Appl Soil Phys Surv Geophys*. 1998;19:23–72.
10. Fatt M. The network model of porous media: I. capillary pressure characteristics. *Pet Trans*. 1956;207:142–164.
11. Chatzis I, Dullien FAL. The modelling of mercury porosimetry and relative permeability of mercury in sandstones using percolation theory. *Int Chem Eng*. 1985;25:47–66.
12. Lapidus L, Lane AM, Ng KM, Conner WC. Interpretation of mercury porosimetry data using a pore-throat network model. *Chem Eng Commun*. 1985;38:2–33.
13. Tsakiroglou CD, Payatakes AC. A new simulator of mercury porosimetry for the characterization of porous materials. *J Colloid Interface Sci*. 1990;137:315–339.
14. Mata VG, Lopes JCB, Dias MM. Porous media characterization using mercury porosimetry simulation. I. Description of the simulator and its sensitivity to model parameters *Ind Eng Chem Res*. 2001;40:3511–3522.
15. Diaz CE, Chatzis I, Dullien FAL. Simulation of capillary pressure curves using bond correlated site percolation on a simple cubic network. *Transport Porous Med*. 1987;2:215–240.
16. Kantzas A, Chatzis I. Application of the preconditioned conjugate gradients method in the simulation of relative permeability properties of porous media. *Chem Eng Commun*. 1988;69:169–189.
17. Koplik J, Lasseter TJ. Two-phase flow in random network models of porous media. *Soc Pet Eng J*. 1985;25:89–100.
18. Dias MM, Payatakes AC. Network models for two-phase flow in porous media. I. immiscible microdisplacement of non-wetting fluids. *J Fluid Mech*. 1986;164:305–336.
19. Lenormand R, Touboul E, Zarcone C. Numerical models and experiments on immiscible displacements in porous media. *J Fluid Mech*. 1988;189:165–167.
20. Constantinides GN, Payatakes AC. Network simulation of steady-state two-phase flow in consolidated porous media. *AIChE J*. 1996; 42:369–382.
21. Constantinides GN, Payatakes AC. A three dimensional network model for consolidated porous media. *Basic Stud Chem Eng Commun*. 1989;81:55–81.
22. Martins AA, Laranjeira PE, Lopes JCB, Dias MM. Network modelling of flow in a packed bed. *AIChE J*. 2007;53:91–107.
23. Saffman PG. Dispersion in flow through a network of capillaries. *Chem Eng Sci*. 1959;11:125–129.
24. Sahimi M, Hughes BD, Scriven LE, Davis HT. Dispersion in flow through porous media - I: one phase flow. *Chem Eng Sci*. 1986;41: 2103–2122.
25. Koplik J, Redner S, Wilkinson D. Transport and dispersion in random networks with percolation disorder. *Phys Rev A: At Mol Opt Phys*. 1988;37:2619–2636.
26. Andrade JS. Hydrodynamic dispersion in binary packings of spheres. *Physica A: Stat Mech Appl*. 1993;199:431–444.
27. Avilés BE, LeVan MD. Network models for nonuniform flow and adsorption in fixed beds. *Chem Eng Sci*. 1991;46:1935–1944.
28. Russell BP, LeVan MD. Nonlinear adsorption and hydrodynamic dispersion in self-similar networks. *Chem Eng Sci*. 1997;52:1501–1510.
29. Alvarado V, Davis HT, Scriven LE. Effects of pore-level reaction on dispersion in porous media. *Chem Eng Sci*. 1997;52:2865–2881.
30. Suchomel BJ, Chen BM, Allen MB. Network model of flow, transport and biofilm effects in porous media. *Transport Porous Med*. 1998;30:1–23.
31. Meyers JJ, Liapis AI. Network modelling of the intraparticle convection and diffusion of molecules in porous particles packed in a chromatographic column. *J Chromatogr A*. 1998;827:197–213.
32. Meyers JJ, Liapis AI. Network modelling of the convective flow and diffusion of molecules adsorbing in monoliths and in porous particles packed in a chromatographic column. *J Chromatogr A*. 1999; 852:3–23.
33. Davdar M, Sohrabi M, Sahimi M. Pore network model of deactivation of immobilized glucose isomerase in packed bed reactors. I. Two-dimensional simulations at the particle level. *Chem Eng Sci*. 2001;56:2803–2819.
34. Davdar M, Sahimi M. Pore network model of deactivation of immobilized glucose isomerase in packed bed reactors. II. Three-dimensional simulation at the particle level. *Chem Eng Sci*. 2002;57:939–952.
35. Davdar M, Sohrabi M, Sahimi M. Pore network model of deactivation of immobilized glucose isomerase in packed bed reactors. III. Multiscale modelling. *Chem Eng Sci*. 2003;58:4935–4951.
36. Li L, Peters CA. Upscaling geochemical reaction rates using pore-scale network modelling. *Adv Water Resour*. 2006;29:1353–1370.
37. Malstrom ME, Destouni G, Martinet P. Modelling expected solute concentration in randomly heterogenous flow systems with multicomponent reactions. *Environ Sci Technol*. 2006;38:2673–2679.
38. Deans HA, Lapidus LA. Computational model for predicting and correlating the behaviour of fixed-bed reactors. I. Derivation of model for nonreactive systems. *AIChE J*. 1960;6:656–663.
39. Schnitzlein K, Hofmann H. An alternative model for catalytic fixed bed reactors. *Chem Eng Sci*. 1987;42:2569–2577.

40. Khang SJ, Levenspiel O. New scale-up and design method for stirrer agitated batch mixing vessels. *Chem Eng Sci*. 1976;31:569–577.
41. Mann R, Knysh P. Utility of interconnected networks of backmixed zones to represent mixing in a closed stirred vessel. *Inst Chem Eng Symp Ser*. 1984;89:127–145.
42. Mann R. Gas-liquid stirred vessel mixers: towards an unified theory based on network of zones. *Trans Inst Chem Eng*. 1986;64:23–34.
43. Zahradník J, Mann R, Fialová M, Vlaev D, Vlaev SD, Lossev V, Seichter PA. Networks-of-zones analysis of mixing and mass transfer in three industrial bioreactors. *Chem Eng Sci*. 2001;56:485–492.
44. Brucato A, Ciofalo M, Grisafi F, Tocco R. On the simulation of stirred tank reactors via computational fluid dynamics. *Chem Eng Sci*. 2000;55:291–302.
45. Wang YD, Mann R. Partial segregation in stirred batch reactors: effect of scale-up on the yield of a pair of competing reactions. *Chem Eng Res Des*. 1992;70:282–290.
46. Rahimi M, Mann R. Macro-mixing, partial segregation and 3-D selectivity fields inside a semi-batch stirred reactor. *Chem Eng Sci*. 2001;56:763–769.
47. Moulijn JA, Stankiewicz A, Grievink J, Gorak A. Process intensification and process system engineering: a friendly symbiosis. *Comput Chem Eng*. 2008;32:3–11.
48. Laranjeira PEMSC.NETMIX® Static Mixer, Modelling, CFD and Experimental Characterization, PhD Dissertation, Universidade do Porto, Porto, Portugal, 2006.
49. Martins AA, Lopes JCB, Dias MM. Mass Transport in Packed Bed Reactors Using Network Models. CD-ROM Abstract O5.2003, ECCE-44th European Congress of Chemical Engineering, Granada, Spain, September, 2003.
50. Lopes JCB, Laranjeira PE, Dias MM, Martins AA. Network Mixer and Related Mixing Process. PCT WO 2005/077508 A1, August 2005.
51. Laranjeira PE, Martins AA, Lopes JC, Dias MM. Mixing and Reaction in Porous Media: Modelling using Pore Networks. CHEMPOR'2001, Aveiro, Portugal, 2001.
52. Martins AA, Lopes JCB, Dias MM. Mass Transport in Packed Bed Reactors Using Network Models, ECCE-44th European Congress of Chemical Engineering, Granada, Spain, 2003.
53. Wen CY, Fan LT. *Models for Flow Systems and Chemical Reactors*. New York: Marcel Dekker, 1975.
54. Levenspiel O. *Chemical Reaction Engineering*. New York: Wiley, 1972.
55. Danckwerts PV. Continuous-flow systems: distribution of residence times. *Chem Eng Sci*. 1953;2:1–13.
56. Coker AK. *Modelling of Chemical Kinetics and Reactor Design*. Boston: Gulf Publishing Company, 2001.
57. Danckwerts PV. The Definition and Measurement of Some Characteristics of Mixtures. *Appl Sci Res*. 1952;3:279–296.
58. Baldyga J, Bourne JR. *Turbulent Mixing and Chemical Reactions*. Chichester, UK: Wiley, 1999.
59. Bourne JR, Kozicki F, Rys P. Mixing and Fast Chemical Reaction - I. Test Reactions to Determine Segregation. *Chem Eng Sci*. 1981;36:1643–1648.
60. Bourne JR. The Characterization of Micromixing Using Fast Multiple Reactions. *Chem Eng Commun*. 1982;16:79–90.

Manuscript received May 14, 2008, and revision received Dec. 12, 2008.